by

T. B. Cox and J. R. Low, Jr.

NASA Technical Report No. 3
on Research Grant NGR 39-087-003 (May 1972)

METALS RESEARCH LABORATORY
CARNEGIE INSTITUTE OF TECHNOLOGY

Carnegie-Mellon University

PITTSBURGH, PENNSYLVANIA

ERRATA FOR

Investigation of the Plastic Fracture
of High Strength Steels

by

T. B. Cox and J. R. Low, Jr.

NASA Technical Report No. 3
on Research Grant NGR 39-087-003 (May 1972)

Please note that in Table III, page 20, the values for the volume fraction of non-metallic inclusions $f_v(\%)$ in the commercial and high purity AISI 4340 alloys were incorrectly reported, respectively, as 0.80 ± 0.42 and 0.21 ± 0.06. The correct values are as follows:

	$f_v(\%)$
Commercial AISI 4340	0.10 ± 0.05
High Purity AISI 4340	0.03 ± 0.01

October 1972

National Aeronautics and Space Administration
Research Grant NGR 39-087-003

Investigation of the Plastic Fracture of High Strength Steels

by

T. B. Cox and J. R. Low, Jr.

TR-#3

Department of Metallurgy and Materials Science
Carnegie-Mellon University
Pittsburgh, Pennsylvania 15213

NASA Technical Report No. 3

May 1972

This investigation was made possible by a Research Grant from the National Aeronautics and Space Administration

INTRODUCTION

The brittle fracture of many of the high strength ferrous alloys occurs by plastic fracture,[1] sometimes referred to as dimpled rupture in reference to the microscopic appearance of the fracture surface. The plastic fracture process in high strength alloys generally may be divided into three stages: void nucleation, void growth and void coalescence. Several investigations [2,3,4] have demonstrated that the nucleation of voids in high strength steels is caused by second-phase particles, including sulfides, carbides and nitrides, depending upon the exact alloy. Since the subsequent growth and coalescence of these voids leads to fracture, the exact nature of the second phase particles and their spacial distribution and density in the ferrous matrix presumably have a great influence on the fracture toughness of the high strength steels.

In order to better understand the plastic fracture process in high strength steels and thereby suggest means of improving the toughness of these alloys, the current investigation has been undertaken. Two generic types of high strength steels are being investigated, a quenched and tempered grade and a maraging grade, to provide comparison between two different matrix microstructures. In addition, each type of steel is being investigated in commercial grade purity and in special melted high purity form, low in residual and impurity elements. The specific alloys being studied are AISI 4340 and 18 Ni, 200 grade maraging steel, both heat treated to the same yield strength level of approximately 200 ksi.

Work completed to date and reported herein includes:

1. Determination of the chemical compositions, heat treatments and mechanical properties of the four alloys.

2. A quantitative metallographic investigation to define the nature of the non-metallic inclusion populations in the four alloys.

3. A fractographic study to define the fracture surface characteristics of each alloy.

MATERIALS

The commercial purity alloys were both made in regular mill production heats while both high purity alloys were made in special melted laboratory heats. The commercial grade AISI 4340 was produced using an electric furnace process and was provided as one-inch thick plate straight-away rolled. The commercial 18 Ni, 200 grade maraging steel was provided as four-inch thick plate, hot pressed and straight-away rolled from a consumable electrode, vacuum remelted ingot. Both the high purity AISI 4340 and the high purity 18 Ni maraging steel were made from 300 pound vacuum induction melted heats of specially selected charges. The ingots were subsequently cross rolled (approximately one-to-one ratio) to one-inch thick plates. The chemical analyses are presented in Table I. The major differences to be noted are the substantial reductions in the impurity levels when going from the commercial melts to the high purity melts, specifically P, S, N_2 and O_2 in the AISI 4340 and these same impurities in the 18 Ni, 200 grade maraging steel together with C. In addition, the amount of Al is lower in both high purity melts as compared with the commercial melts and in the 18 Ni, 200 grade maraging alloy, high purity melting results in reduction of Mn and Si levels.

Since it is desired to investigate the fracture behavior of these alloys at approximately the same strength level, they were given heat treatments designed to produce yield strengths close to 200 ksi. Both AISI 4340 alloys were austenitized at 843°C (1550°C) for one hour and oil quenched. Due to the differences in carbon contents, the tempering treatments were different with the commercial AISI 4340 being tempered

TABLE I

Composition of High Strength Steels

(Weight Percent)

	Commercial AISI 4340	High Purity AISI 4340	Commercial 18 Ni	High Purity 18 Ni
C	0.43 ± 0.01	0.38 ± 0.01	0.021 ± 0.004	0.002 ± 0.002
Mn	0.78 ± 0.02	0.71 ± 0.02	0.04 ± 0.01	< 0.02 ± 0.01
P	0.010 ± 0.001	0.001 ± 0.001	0.003 ± 0.001	0.002 ± 0.001
S	0.013 ± 0.001	0.004 ± 0.001	0.008 ± 0.001	0.004 ± 0.001
Si	0.27 ± 0.02	0.29 ± 0.02	0.04 ± 0.01	< 0.03 ± 0.02
Ni	1.73 ± 0.02	1.81 ± 0.02	18.3 ± 0.1	18.1 ± 0.1
Cr	0.76 ± 0.02	0.80 ± 0.02	< 0.04 ± 0.02	0.05 ± 0.02
Mo	0.25 ± 0.01	0.25 ± 0.01	4.23 ± 0.05	4.16 ± 0.05
Al(total)	0.049 ± 0.003	0.023 ± 0.002	0.080 ± 0.002	0.062 ± 0.002
Co	---	0.010 ± 0.01	7.85 ± 0.1	8.03 ± 0.1
Ti	---	< 0.005 ± 0.002	0.19 ± 0.01	0.23 ± 0.01
N_2	0.008 ± 0.001	0.003 ± 0.001	0.005 ± 0.001	0.004 ± 0.001
O_2	50 ± 10 ppm	23 ± 3 ppm	30 ± 10 ppm	23 ± 3 ppm
Fe	Balance	Balance	Balance	Balance

at 435°C (815°F) for one hour and air cooled while the high purity alloy was tempered at 427°C (800°F) for one hour and air cooled. The specially produced high purity 18 Ni, 200 grade maraging steel was solution annealed at 843°C (1550°F) for one hour and water quenched, then aged for three hours at 454°C (850°F) and air cooled. The commercial grade 18 Ni steel was solution annealed at 899°C (1650°F) for two and one-half hours and air cooled, followed by aging at 446°C (835°F) for six hours and air cooled. The differences in heat treatments for the maraging steels were necessitated by the large difference in plate thicknesses, i.e., one verses four inches.

The mechanical properties resulting from these heat treatments are given in Table II. The tensile data were determined using standard geometry, smooth, round tensile specimens. The fracture toughness testing was all performed at NASA Lewis Research Center. The value of K_{Ic} for the commercial purity 18 Ni, 200 grade maraging steel was obtained by interpolation of the data of Fisher and Repko[5] who used the same plate material used in this investigation for 3.9 inch thick bend specimens. The other K_{Ic} values were determined by W. F. Brown and M. H. Jones using compact tension specimens. All fracture toughness tests were performed in accordance with ASTM standard E 399-70T. The fracture toughness specimens were tested in the W R orientation (notched through the plate thickness with the direction of crack propagation in the primary rolling direction). The tensile bars were taken in the same orientation.

Reference to Table II reveals that the yield strengths of the alloys are in the general range of 200 ksi. Care was taken to match yield

TABLE II

Room Temperature Mechanical Properties of High Strength Steels

(all values represent means of duplicate tests)

	Commercial AISI 4340	High Purity AISI 4340	Commercial 18 Ni	High Purity 18 Ni
Yield Strength 0.2% Offset (ksi)	204.8	204.6	193.5	189.9
Ultimate Tensile Strength (ksi)	221.6	218.0	197.7	198.5
True Strain to Fracture	0.287	0.515	0.747	1.005
Strain Hardening Exponent	0.032	0.029	0.062	0.055
Fracture Toughness K_{Ic} (ksi/in)	67.9	97.2	113.0	149.1*

* K_Q, invalid test due to undersized specimens. K_{Ic} believed to be substantially higher, ~ 180 ksi/in.

strengths within a given alloy system, although the general level of yield strength is about 15 ksi greater in the AISI 4340 alloys than in the maraging steels. This difference was the result of several factors. The yield strength of approximately 190 ksi realized for the high purity 18 Ni, 200 grade maraging steel represents the maximum strength attainable in this particular heat. It was decided not to temper the AISI 4340 to this same strength level since past experience indicated that it would be impossible to get a valid K_{Ic} measurement in the one-inch thick high purity plate of AISI 4340 at this low strength. The values of true strain to fracture in Table II indicate that the ductility of these alloys is substantially improved by high purity melting and that the general level of ductility is higher for the maraging steels than for the quenched and tempered AISI 4340 alloys. The same observation may be made for the fracture toughness values. The level of fracture toughness is greater in the maraging steels than in the AISI 4340 steels even when considering the difference in yield strength. Within a given alloy system, reduction of the impurity levels improves the fracture toughness.

Typical optical micrographs of polished and etched sections of the four alloys are presented in Figure 1. The AISI 4340 alloys are etched in a saturated solution of picric acid in ethyl alcohol and the maraging steels are etched in a concentrated aqueous solution of ferric chloride and hydrochloric acid. The AISI 4340 alloys both exhibit a very fine grain size characteristic of quenched and tempered martensitic structures. There is some evidence of alloy banding and the presence of non-metallic inclusions in the structures. The maraging steels exhibit a very fine structure

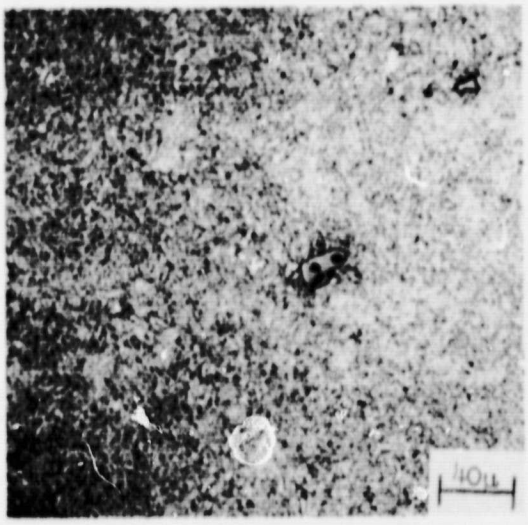

Commercial AISI 4340

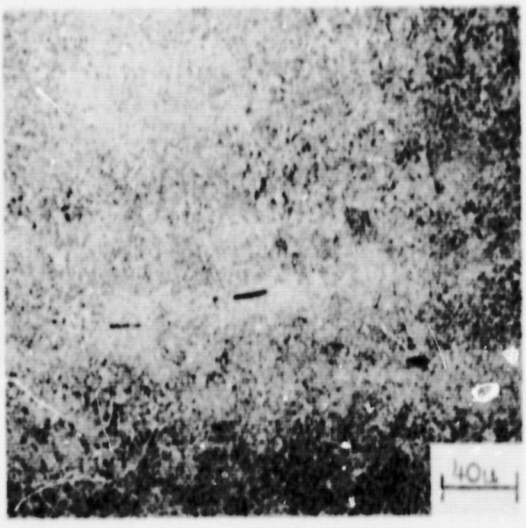

High Purity AISI 4340

Primary

Rolling Direction

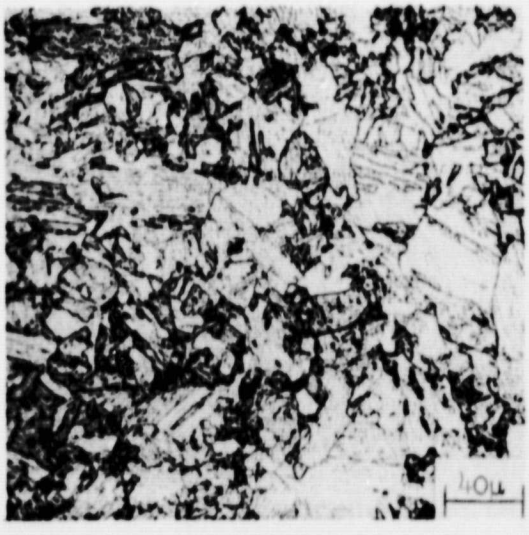

Commercial 18 Ni Maraging

High Purity 18 Ni Maraging

Figure 1 Optical Micrographs of Polished and Etched Sections of High Strength Steels

within the prior austenite boundaries which are delineated by the etch. As should be expected, the higher austenitizing temperature used for the commercial alloy has resulted in a slightly larger austenite grain size. Evidence of alloy banding is also prevalent in the maraging micrographs, but the etching has obscured the non-metallic inclusions present in the microstructures.

The fine internal structures of these martensitic steels are shown in the transmission electron micrographs of Figure 2. Included in the figure are micrographs of thin foils from the two high purity alloys which are representative of the structures in the two families of steels. The thin foils were produced by cutting sections approximately 0.5 mm (20 mils) thick using a water cooled cut-off wheel. These sections were then hand ground on silicon carbide papers using water cooling to a thickness of approximately 0.1 mm (4-5 mils). Final thinning was accomplished electrolytically using a thinning solution of chromium trioxide in glacial acetic acid. As is seen in Figure 2a, the quenched and tempered AISI 4340 alloys exhibited an acicular grain structure, high dislocation density and evidence of carbide precipitation generally at the martensite platelet boundaries. These observations are in agreement with previous investigators of this same alloy, tempered to the same strength level.[6] The micrograph of the maraging steel in Figure 2b exhibits a less acicular grain structure than the AISI 4340, a high dislocation density and a fine ribbon-like precipitate thought to be Ni_3Mo. These observations also coincide with those made by other investigators [7] of maraging structures.

a. AISI 4340

b. 18 Ni Maraging

Figure 2 Transmission Electron Micrographs of High Strength Steels

INCLUSION IDENTIFICATION

In order to define the exact nature of the non-metallic inclusions in the four alloys, a metallographic investigation was undertaken. For each of the four alloys, metallographic sections were examined from each of three orthogonal directions, the axes being defined by the rolling directions and the through thickness direction in each of the plates.

Polished sections through both of the AISI 4340 alloys revealed that the predominate inclusion type in these alloys appeared as a gray ellipse in each of the three perpendicular directions. An example of this inclusion type is shown in Figure 3a. The sizes of the ellipses varied from view to view, being much elongated in the rolling direction. In many instances a smaller irregular black particle was found within the large gray ellipse, as is illustrated in Figure 3a. The only differences noted between the non-metallic inclusions in the high purity AISI 4340 and those in the commercial alloy were the size and axial ratios. Generally, the inclusions were observed to be larger in the commercial AISI 4340, and the major axes of the ellipses seemed more elongated in the rolling direction of the commercial alloy. Since these inclusions are oriented in the rolling directions, they were undoubtedly plastically deformed during the hot rolling operation. The exaggeration of the major axes of the ellipses in the commercial alloy as compared to the high purity plate reflect the fact that the high purity plate was cross-rolled, while the commercial plate was straight-away rolled. Based upon their appearance in the optical microscope and comparison with descriptions from previous inclusion studies,[8]

15μ

a. AISI 4340

Primary
Rolling Direction

15μ

b. 18 Ni Maraging

Figure 3 Optical Micrographs of Inclusions in High Strength Steels

these gray, ellipsoidal inclusions in the AISI 4340 alloys were tentatively identified as manganese sulfides (MnS); and the black particles internal to the sulfides as some product of the deoxidation process upon which the sulfides are nucleated.

Figure 3b presents a typical example of the most prevalent non-metallic inclusion type in the 18 Ni, 200 grade maraging alloys. In all three orthogonal views from both alloys, the inclusions appeared as sections of cubes and exhibited a pink color in the optical microscope. The cubes did not appear to have been plastically deformed during the hot rolling operation, and the cubic sections appeared to have approximately the same size distribution in each of the three views of a given alloy. The cubes did appear to be larger in the commercial 18 Ni maraging steel. Comparison of these optical metallographic observations with those of a previous investigation[9] led to a preliminary identification of the inclusions in the maraging alloys as titanium carbo-nitrides (Ti(C,N)).

To ascertain whether or not the preliminary identification of the non-metallic inclusions in the four alloys was correct, specimens of each alloy metallographically polished only through one micron diamond paste were examined by using a scanning electron microscope equipped with an X-ray energy-dispersive analyzer. Comparison of intensities of elemental characteristic X-rays from the inclusions and matrices confirmed the postulated inclusion identifications. The ellipsoidal inclusions in both the commercial and high purity AISI 4340 alloys were found to be richer in manganese and sulfur than the matrix. The small irregular

inclusions upon which the sulfides apparently nucleated were found to contain greater amounts of calcium and aluminum than the matrix in the commercial AISI 4340, suggesting a deoxidation product. (It is impossible to analyze for oxygen using this technique.) Unfortunately, the nucleating particles within the manganese sulfides were too small in the high purity AISI 4340 to provide sufficient volume for analysis. Figure 4 is an example of representative micrographs of a manganese sulfide inclusion in the commercial AISI 4340 alloy. Included are photomicrographs taken in the secondary electron mode and subsequent elemental X-ray scans of the same area. It is seen that the inclusion is rich in manganese and sulfur and that the black nucleating particle is rich in aluminum. The white spots within the black particle and the sulfide are positions where prolonged X-ray counting was done for analysis of the inclusions.

The same procedure was used for analyzing the inclusions in both maraging alloys. A representative example of micrographs taken of a suspected titanium carbo-nitride is presented in Figure 5. Again, the bright spots on the photograph taken in the secondary electron mode are points where prolonged X-ray counting was carried out. The inclusion is richer in titanium than the matrix. Unfortunately, no analyses can be made for carbon or nitrogen using this technique, but the detection of titanium together with their optical appearance strongly indicates that the cuboidal inclusions in the maraging alloys are titanium carbo-nitrides.

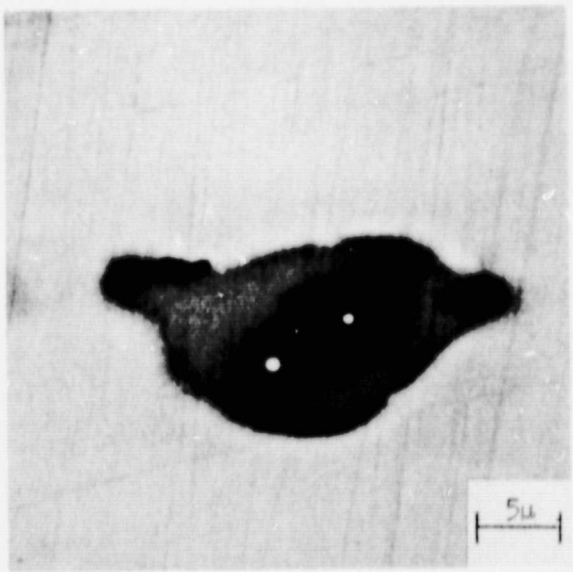

Secondary Electron Mode

X-Ray Scan for Aluminum

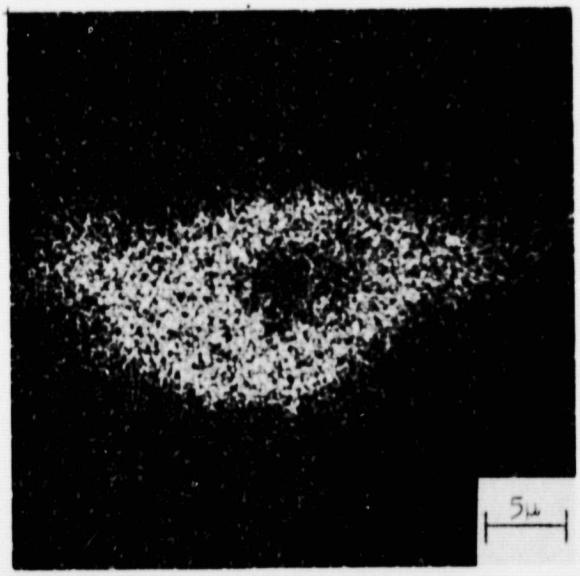

X-Ray Scan for Manganese

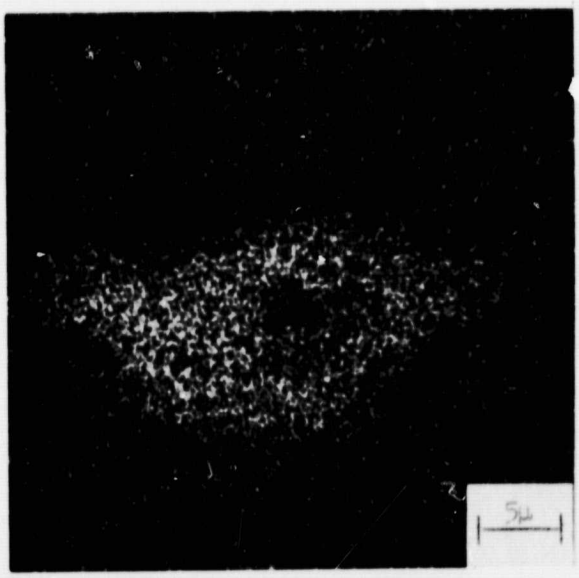

X-Ray Scan for Sulfur

Figure 4 Scanning Electron Micrographs of Inclusion in AISI 4340 Steel

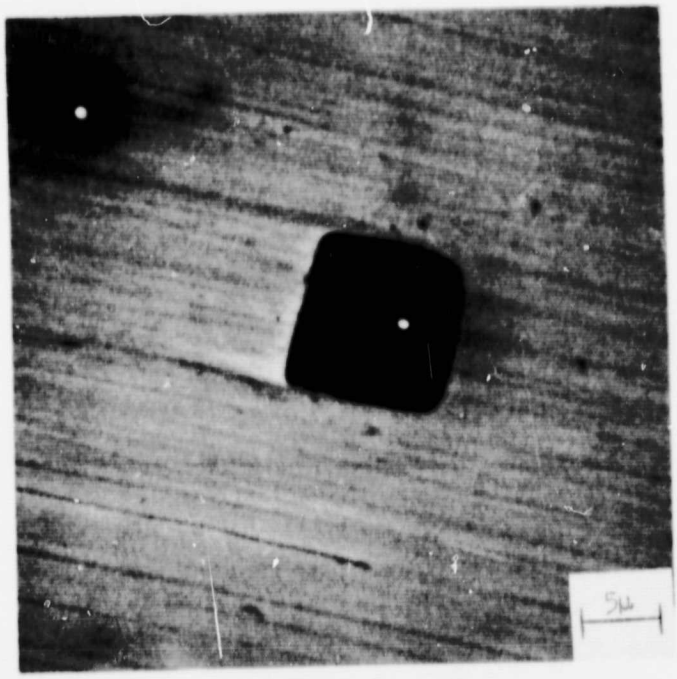

Secondary Electron Mode

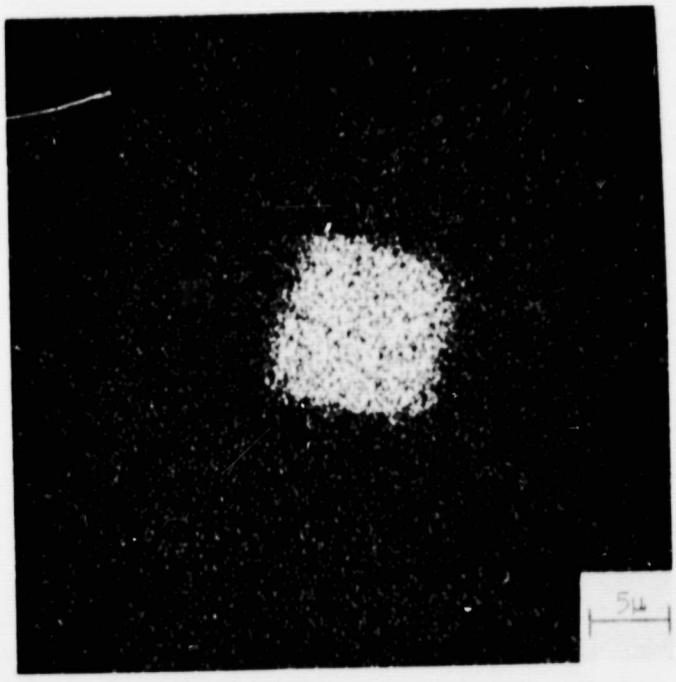

X-Ray Scan for Titanium

Figure 5 Scanning Electron Micrographs of Inclusion in 18 Ni Maraging Steel

QUANTITATIVE METALLOGRAPHY

A quantitative metallographic investigation was undertaken to determine the exact nature of the inclusion populations in the four alloys. Based on the definition of the inclusion shapes indicated above, established quantitative metallographic techniques were used to determine the numbers, spacings and sizes of the inclusions in the alloys. Polished plane sections normal to each of the three orthogonal axes as defined by the rolling directions and plate thicknesses were examined for each alloy. Optical photomicrographs were taken at sixteen predetermined positions on each plane section. The positions were defined by four-point by four-point square arrays on the sections. Photomicrographs were taken at a magnification of 250x and then enlarged to 500x to facilitate counting and measuring of the inclusions in each view. All features which could be identified as inclusions were counted and their dimensions measured.

The manganese sulfide inclusions in the AISI 4340 alloys have the shape of ellipsoids, with their three unequal axes aligned in the orthogonal directions defined by the rolling direction, the cross-rolling direction and the through thickness direction of the plates. The quantitative metallographic analysis for this shape is due to DeHoff and Rhines[10, 11], assuming a constant shape ellipsoid, i.e., the ratio of the axes remains constant. The dimensions of the ellipsoid are defined by the lengths of its three axes: d_1 (along the primary rolling direction), d_2 (along the cross-rolling direction), and d_3 (along the direction through the plate thickness). The number of inclusions per unit area observed on a test section perpendicular

to axis 1 (the primary rolling direction) is given the symbol N_{A1}. Similarly defined are N_{A2} and N_{A3}. Furthermore, Z_{13} is defined as the reciprocal of the length of the axis of those elliptical sections which are seen on plane 1 (normal to the primary rolling direction) with the measurement being made in the three direction (the through thickness direction).

The number of ellipsoidal inclusions per unit volume of material (N_v) is then given by the expression:

$$N_v = \frac{2}{\pi} N_{A3} \overline{Z_{13}}$$

The mean dimensions of the ellipsoidal inclusions ($\bar{d}_1$) are given by:

$$\bar{d}_1 = \frac{\pi}{2} \frac{N_{A1}}{N_{A3} \overline{Z}_{13}}$$

$$\bar{d}_2 = \frac{\pi}{2} \frac{N_{A2}}{N_{A3} \overline{Z}_{13}}$$

$$\bar{d}_3 = \frac{\pi}{2 \overline{Z}_{13}}$$

The titanium carbo-nitrides which are the predominate inclusion type in the 18 Ni maraging alloys have the shape of cubes, approximately of constant size and with no preferred orientation in the matrix. The quantitative metallographic treatment of this shape is due to Hull and Houk[12] and Myers[13]. The number of inclusions per unit area observed on a randum plane is given the symbol N_A, and the number of interceptions

of inclusions per unit length of a test line randomly placed on plane sections is given the symbol N_L.

The number of cuboidal inclusions per unit volume of material (N_V) is then given by the expression:

$$N_V = \frac{2N_A^2}{3N_L}$$

The true dimension of the cube edges (a) is given by:

$$a = \frac{N_L}{N_A}$$

For both types of inclusion shape, the average center-to-center distance ($\bar{\lambda}$) between the nearest neighbor inclusions in a unit of volume is given by an expression first derived by Hertz[14]:

$$\bar{\lambda} = 0.554\, N_V^{-1/3}$$

The results of the quantitative metallographic study are summarized in Table III. The limits given for each reported value represent plus and minus one standard deviation (approximately 70 percent confidence limits). It should be noted from the table that the number of inclusions per unit volume is greater for the high purity alloys than for the commercially produced plates, but that the inclusion sizes and volume fractions (f_V) are substantially larger in the commercial alloys. The center-to-center spacing of inclusions follows the inverse relation of the number per unit volume, namely, the interparticle spacings are greater in the

TABLE III

Results of Quantitative Metallographic Investigation of High Strength Steels

	Commercial AISI 4340	High Purity AISI 4340	Commercial 18 Ni Maraging	High Purity 18 Ni Maraging
$\left(\frac{N_V \text{ inclusions}}{cm^3}\right)$	$4.9 \times 10^6 \pm 2.6 \times 10^6$	$6.8 \times 10^6 \pm 4.6 \times 10^6$	$2.9 \times 10^6 \pm 1.5 \times 10^6$	$5.4 \times 10^6 \pm 5.1 \times 10^6$
$\bar{d}_1$ or a (μ)	9.7 ± 5.8	4.5 ± 4.1	8.6 ± 6.4	3.0 ± 3.8
$\bar{d}_2$ (μ)	7.3 ± 6.3	4.9 ± 4.2	---	---
$\bar{d}_3$ (μ)	5.5 ± 1.4	3.3 ± 0.2	---	---
$\bar{\lambda}$ (μ)	33 ± 6	29 ± 7	39 ± 7	32 ± 10
f_v (%)	0.80 ± 0.42	0.21 ± 0.06	0.18 ± 0.20	0.08 ± 0.11

commercial alloys than in the high purity alloys. As may be seen from the results, the variability of the various measurements is quite high. However, treatment of the data using the t statistic shows that the above conclusions concerning numbers, sizes and spacings of the inclusions are statistically meaningful with 90 percent confidence.

Analysis of the data for the AISI 4340 alloys reveals that the number of inclusions per unit volume in the high purity alloy is greater by at least 0.2×10^6 inclusions/cm^3 than in the commercial grade plate. Similarly with 90 percent confidence, the average inclusion size is larger in the commercial alloy with $\bar{d}_1$ at least 2.9μ greater than in the high purity alloy. Likewise, $\bar{d}_2$ and $\bar{d}_3$ are at least 0.1μ and 1.7μ greater, respectively, in the commercial AISI 4340 than in the high purity melt. It was also determined that $\bar{\lambda}$ is at least 1.7μ larger in the commercial alloy than in the high purity alloy, and that f_v is at least 0.45 percent greater in the commercial alloy.

Similar statistical treatment of the data for the 18 Ni, 200 grade maraging steels shows that N_v of the high purity melt is at least 0.8×10^6 inclusions/cm^3 greater than N_v for the commercial alloy, again with 90 percent confidence. The size of the titanium carbo-nitride cube edge is at least 3.2μ greater in the commercial alloy while $\bar{\lambda}$ also is at least 3μ greater in the commercial alloy than in the high purity plate of 18 Ni, 200 grade maraging steel. Due to the large variability in the data, no statistical difference in f_v could be established between the high purity and commercial grades of maraging steel.

FRACTOGRAPHY

A fractographic study was carried out on the four alloys to define the nature of the fracture surfaces. Two stage, cellulose acetate-platinum shadowed carbon replicas were taken from the areas of fast fracture initiation on the K_{Ic} fracture surfaces and from the centeral areas of normal rupture on the tensile fracture surfaces for each of the alloys. K_{Ic} fracture surfaces were not available for the commercial 18 Ni, 200 grade maraging steel at the 200 ksi yield strength level, thus only tensile fractures were examined for this alloy. The replicas were examined in the electron microscope, and it was found that the features on the fracture surfaces were qualitatively the same for each of the two fracture tests (K_{Ic} and tension) of any given alloy. Examples of representative fractographs taken of replicas of the central regions of the fracture surfaces of tensile specimens from each of the four alloys are presented in Figures 6 through 9.

Examination of the 18 Ni maraging fractographs in Figures 6 and 7 reveals the fracture surfaces to be almost completely covered by large dimples approximately 10-20μ in diameter. At the positions marked "X" on the fractographs, examples of impressions of carbo-nitride particles may be seen at the bottoms of dimples. The particular carbo-nitride marked "Y" in Figure 7 exhibits a clear cleavage fracture pattern, suggesting that the associated dimple was nucleated by the separation of the halves of the fractured non-metallic inclusion. The other large dimples were also presumably nucleated at carbo-nitride particles, which are either seen within the dimples or have failed to be replicated for some reason.

(Carbo-Nitrides indicated by X; Deformation Markings indicated by R)

Figure 6 Electron Fractograph of Two-Stage Replica from Central Region of Tensile Fracture in Commercial 18 Ni Maraging Steel

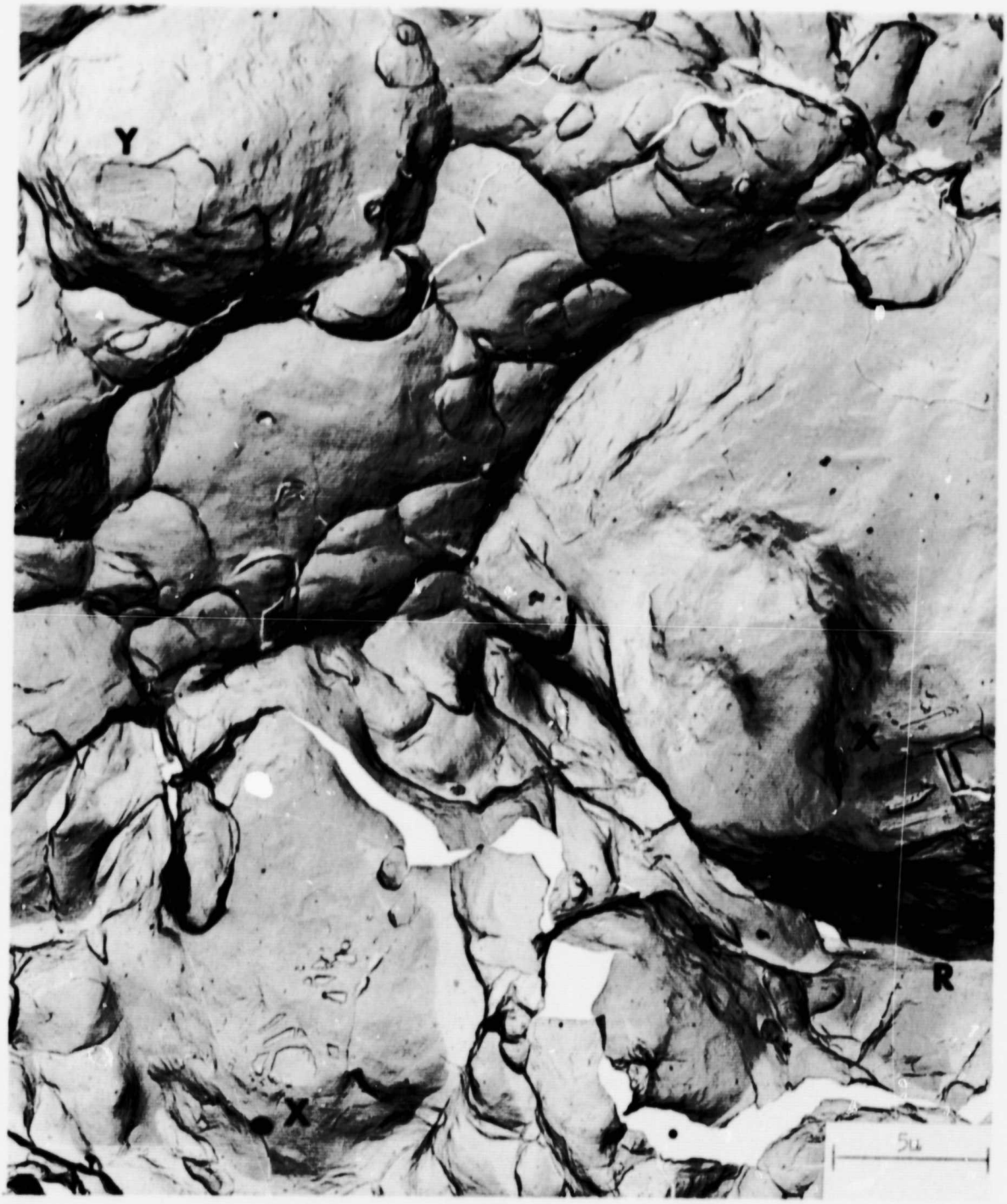

(Carbo-Nitrides indicated by X; Cleavage Fracture Pattern on Carbo-Nitride indicated by Y; Deformation Markings indicated by R)

Figure 7 Electron Fractograph of Two-Stage Replica from Central Region of Tensile Fracture in High Purity 18 Ni Maraging Steel

At the position marked "R" in Figures 6 and 7, evidence of surface rumpling of the dimple walls is seen. These wavy features are reminiscent of the intense deformation markings on the free surfaces of tensile specimens, which have been strained well into the plastic region. The implication is that the dimple walls were, in fact, free surfaces during a major portion of the plastic deformation of the matrix. It has been observed that these intense deformation markings are more numerous and pronounced for the more ductile high purity 18 Ni, 200 grade maraging alloy than for the commercial alloy, as may be seen by comparison of Figures 6 and 7.

Representative fractographs of the tensile fractures observed in the AISI 4340 alloys are presented in Figures 8 and 9. Each of these fractographs is composed of a large dimple 5-15μ in diameter marked with the letter "L" in the figures with the remainder of the area of each fractograph covered with very fine dimples one-to-two orders of magnitude smaller. No fundamental differences between the fractures of the high purity and commercial AISI 4340 alloys could be discerned from their fracture surfaces. Both alloys exhibit extensive surface rumpling on the large dimple walls as was observed in the maraging steels. Careful examination of the areas of fine dimples shows that many of these small dimples contain the impression of a nucleating particle. Likewise, the points marked "X" within the large dimples are most probably the impressions of the nucleating particles for the large dimples. Although the replicated shapes of these particles are not distinctive, their general sizes correspond with those of the manganese sulfide particles identified as the predominate non-metallic inclusions in these AISI 4340 steels.

(Large Dimple indicated by L; Nucleating Particle indicated by X)

Figure 8 Electron Fractograph of Two-Stage Replica from Central Region of Tensile Fracture in Commercial AISI 4340 Steel

(Large Dimple indicated by L; Nucleating Particle indicated by X)

Figure 9 Electron Fractograph of Two-Stage Replica from Central Region of Tensile Fracture in High Purity AISI 4340 Steel

In a further attempt to understand the relation between the nonmetallic inclusions in these alloys and the features on the fracture surfaces, a series of quantitative measurements of dimple spacings were made on the fractographs. The procedure followed was to consider the fracture surfaces as plane sections and the dimples to be analogous to grains, such that measurements made were those generally associated with the determination of the average linear distance across a grain as given by Smith[15]:

$$\bar{D} = L/N$$

where L is the length of test line traversing the test section, and N is the number of cell boundaries intersected by the length of test line. This treatment of the rough fracture as if it were a flat surface obviously introduces error, but should give a first approximation to the average diameter of the dimples or, of more interest, the treatment provides an approximation to the average center-to-center spacing of the dimples. Measurements were made on both K_{Ic} and tensile fracture surfaces to provide a quantitative comparison between the fractures from the two tests for each alloy. Extensive use was made of stereographic pairs of fractographs to better facilitate accurately distinguishing the boundaries between dimples. The results of the measurements from the fractographs are presented in Table IV, together with a tabulation of the average inclusion spacings determined earlier by quantitative metallography to permit ready comparison. All limits on the data represent plus and minus one standard deviation.

The results in Table IV seem to point to a correlation between the average inclusion spacing as determined by quantitative metallography

TABLE IV

Approximations of Dimple Spacings on
Fracture Surfaces of High Strength Steels

	Commercial AISI 4340	High Purity AISI 4340	Commercial 18 Ni Maraging	High Purity 18 Ni Maraging
$\bar{\lambda}$ Spacing of Inclusions from Polished Sections (μ)	33 ± 6	29 ± 7	39 ± 7	32 ± 10
$\bar{D}$ Approximate Spacing of Large Dimples on K_{Ic} Fractures (μ)	18 ± 7	24 ± 6	-	14 ± 3
$\bar{D}$ Approximate Spacing of Large Dimples on Tensile Fractures (μ)	23 ± 11	16 ± 6	26 ± 14	17 ± 5
$\bar{D}$ Approximate Spacing of Small Dimples on K_{Ic} Fractures	0.3 ± 0.1	0.6 ± 0.2	-	-
$\bar{D}$ Approximate Spacing of Small Dimples on Tensile Fractures (μ)	0.4 ± 0.1	0.4 ± 0.2	-	-
Fraction of Fracture Surface Covered by Small Dimples (%)	91.2 ± 0.4	97.0 ± 0.2	~0	~0

and the approximation of the large dimple spacings. The reasonable agreement between these measurements for each alloy is remarkable when considering the approximations made in the determination of dimple spacings. These results coupled with the frequent association of large dimples and inclusions on the fracture surfaces as shown by the fractographs strongly suggest that the large dimples are the result of void initiation at the non-metallic inclusions. One more point should be made concerning the data presented in Table IV. The approximate values of large dimple spacings determined from the K_{Ic} and tensile fracture surfaces are essentially the same for the two tests for any given alloy. Good agreement is also found between the small dimple spacings from K_{Ic} and tensile fractures in the AISI 4340 alloys. This correlation confirms the previous observation that the fracture surface features in the region of fast fracture initiation in K_{Ic} specimens are the same as those from the central region of normal rupture in the round tensile test for these alloys. Thus, it is suggested that the initial or critical processes which lead to fracture are similar for the two tests in these particular alloys.

The major difference between the fracture surfaces of the 18 Ni, 200 grade maraging steels and the AISI 4340 steels is the much greater fraction of the fracture surfaces of the AISI 4340 steels covered by very fine dimples approximately half a micron in diameter. Using a point counting technique outlined by Underwood[16] and assuming again that the fracture surfaces were flat, it was determined that the fraction of the area of K_{Ic} fracture surfaces covered by small dimples was 91.2 ± 0.4 percent for the commercial AISI 4340 and 97.0 ± 0.2 percent for the high purity AISI 4340. Although there is evidence of a few small dimples on the

18 Ni, 200 grade maraging fracture surfaces (see Figures 6 and 7), the areas of small dimples were not extensive enough to measure a statistically significant area fraction for the maraging alloys. The maraging fracture surfaces considered as a whole had approximately 100 percent area fraction of large dimples.

The sizes of the small dimples on the AISI 4340 fracture surfaces and the sizes of the impressions of nucleating particles within them suggest that the small dimples are nucleated on carbide particles in the quenched and tempered martensitic structure. In order to determine the nucleating particles for these fine dimples, a series of extraction replicas were taken from tensile fracture surfaces of both AISI 4340 alloys. The replicas were made by shadowing the actual fracture surfaces with platinum from an angle of approximately 45° and then evaporating a heavy coating of carbon onto the fracture surface from directly overhead. The fracture surfaces with carbon and platinum deposits were immersed in a one percent solution of bromine in methyl alcohol for about one minute to attack the matrix and help expose the particles in the bottoms of the dimples. The fractures were then soaked while agitated for several hours in ethyl alcohol to remove all the bromine solution. The central portions of the tensile fractures were then scribed and electropolished in a solution of perchloric acid, ethyl alcohol and glycerol during which the scribed blocks of carbon replica floated off the fracture surfaces. The replicas, after cleaning in ethyl alcohol, were examined in the electron microscope.

The procedure outlined above resulted in the extraction of many fine particles associated with the small dimples on the fracture surfaces

of both commercial and high purity AISI 4340 alloys. An example of an extraction replica taken from the commercial alloy is presented in Figure 10a. Examples of extracted particles are indicated by the arrows on the fractograph. In order to identify the particles, electron diffraction techniques using the electron microscope were employed so that individual particles associated with the small dimples could be examined. The particle marked "C" in Figure 10a is shown at high magnification in Figure 10b, and the selected area electron diffraction pattern from this particle is presented in Figure 10c. The concentric ring pattern about the central spot of the diffraction pattern results from the fine grained polycrystalline platinum deposit used to shadow the replica, while the discrete spots in the pattern result from diffraction from the small single crystal particle extracted from the fracture surface. This latter point was verified using dark field microscopy on all diffracting particles. Several selected area diffraction patterns were taken from particles from both high purity and commercial alloys. Based on a previous investigation,[6] the carbides in these alloys for the particular heat treatment used were thought most probably to be cementite. The calculated lattice spacings of the planes within the extracted particles producing the spot patterns observed were compared with the reported d spacings of cementite from previous investigations.[17,18,19] These results are presented in Table V. The excellent correlation of the lattice spacings of the extracted particles with those of cementite lead to the conclusion that the strengthening carbides in the AISI 4340 alloys must be the nucleating particles for the formation of the small dimples on the fracture surfaces.

a.

b. Particle C Above

c. Selected Area Diffraction of Particle C

Figure 10 Electron Photomicrographs of Extraction Replica from Commercial AISI 4340 Tensile Fracture

TABLE V

Observed d Spacings from Selection Area Diffraction Patterns of Extracted Particles

Observed d Values (Å)	Previously Reported d Values (Å) for Cementite		
	X-Ray[17]	Electron Diffraction[18,19]	hkl
1.03	1.026	1.03	135
1.12	1.123	1.12, 1.13	323
1.34	1.339	-	124
1.52	1.506	1.51	222
1.60	1.582	1.59	123
1.68	1.679	1.67	220
1.86	1.862	1.87, 1.84	202
1.97	1.968	1.96	211
2.09	2.098	-	121
2.23	2.207	-	120
2.55	2.536	2.54	020
2.79	-	2.79	-
3.35	3.358	-	110
3.72	3.75	3.74	101

To further investigate the fracture surface features of these alloys, fractured tensile halves were nickel plated, sectioned longitudinally and two-stage replicas were taken of the fracture profiles at the mid-thickness of each specimen. Each section was polished and lightly etched before replication to delineate the fracture profile and provide a means of observing whether or not the fractures tended to follow microstructural features. Representative micrographs from the two alloy types are presented in Figure 11. Both the high purity and commercial grade materials for each alloy system exhibited the same fracture profile features, but there is evidence that the fracture path is different in the two alloy systems. The fracture profile seen in Figure 11a of an AISI 4340 specimen shows the fracture to be quite irregular and to follow the boundaries of the acicular ferritic structure. This observation of the fracture path following the ferrite boundaries is in agreement with the findings of a previous study[20] of fracture in a plain carbon steel, heat treated to produce a quenched and tempered martensitic structure. In contrast, the fracture profile typical of the 18 Ni, 200 grade maraging steels shown in Figure 11b exhibits no apparent preference of the fracture for following particular microstructural features.

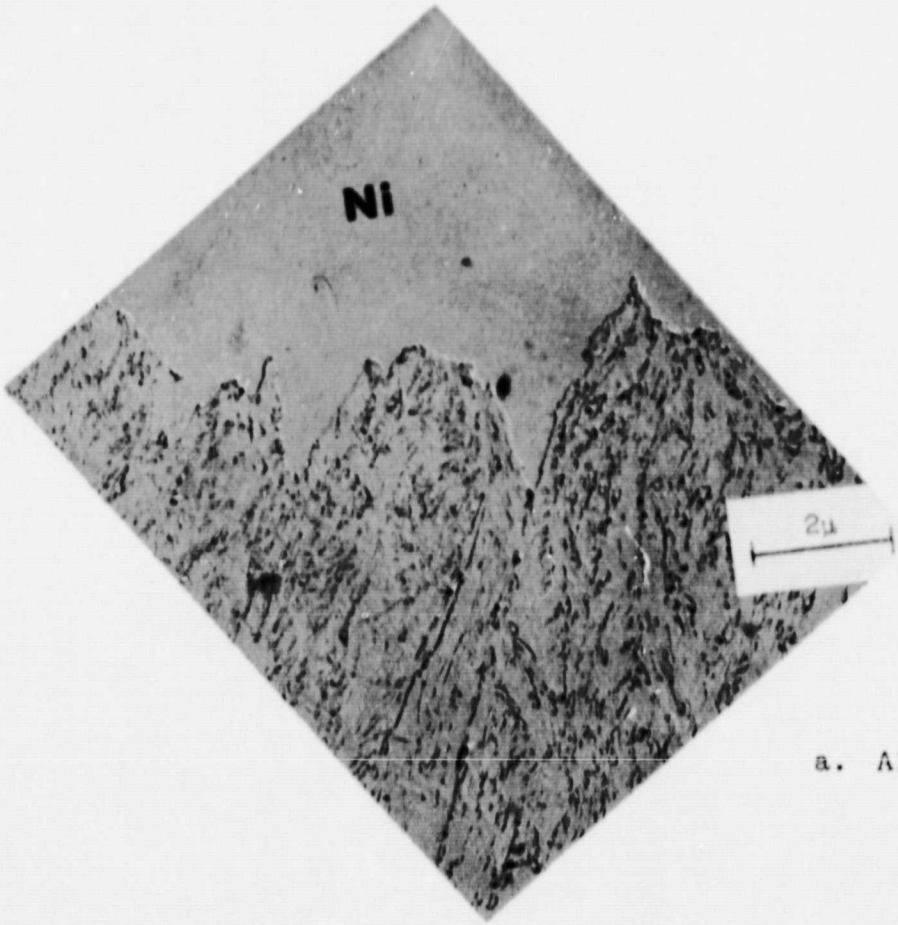

a. AISI 4340

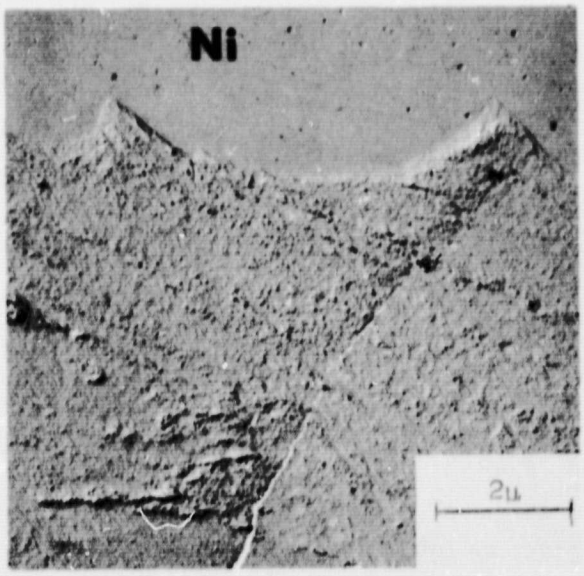

b. 18 Ni Maraging

Figure 11 Profiles of Tension Fractures in High Strength Steels

DISCUSSION

It has been demonstrated above that the non-metallic inclusions in these four alloys serve as nucleation sites for voids during plastic deformation of the steel matrix. Quantitative metallography has shown that the sizes of the inclusions are substantially larger in the commercial alloys than in the high purity heats, but the number of inclusions is greater in the high purity heats. Apparently then, the great improvements in fracture toughness values realized by reducing the impurity levels in each of these two alloy systems is the result of an inclusion size effect; although it should be realized that for these particular heats of steel, the volume fractions of the materials occupied by non-metallic inclusions may also increase as the size of the inclusions increases. It will take further work to define the exact role of the larger inclusions in reducing the toughness. The possibility of the higher stress concentration at the larger particles causing void initiation to occur earlier or the voids to grow faster is a plausible explanation. It is suggested that this question can be answered by studying the void initiation and growth stages in these alloys by straining specimens to various levels, sectioning them and observing the progress of void formation and growth. The experimental technique of sectioning and viewing the voids has been developed during this report period, and work will begin shortly on this aspect of the investigation.

The apparent difference in path taken by the fracture in the two different alloy systems may offer some explanation for the difference in toughness levels between the AISI 4340 alloys and the 18 Ni, 200 grade

maraging alloys. Since the greater portions of the AISI 4340 alloy fracture surfaces are dominated by small dimples nucleated at carbides, it is possible that the direct involvement of the strengthening precipitates in the void nucleation step has a major effect on the toughness level of this quenched and tempered steel. The aspect of the fracture proceeding along the ferritic boundaries in this structure is probably the direct result of the fact that these boundaries are preferred sites for carbide precipitation during tempering,[6] and thus, the density of carbides is greatest there. The strengthening of the maraging steels is by the precipitation of the inter-metallic compound Ni_3Mo, which exists as a much finer dispersion than the cementite in the AISI 4340. Apparently because of their much smaller size, the Ni_3Mo precipitates play no direct roll in the void initiation process other than by their influence on the strength of the matrix. It has been observed recently that by over-aging the maraging steels, it is possible to nucleate voids at the inter-metallic particles.[21] It is felt that the proposed study of the progress of void initiation and growth in these alloys will provide more insight to the reasons for the higher toughness level of the maraging alloys.

CONCLUSIONS

The conclusions which may be drawn from the work completed during this report period include:

1) The fracture toughness values of both the AISI 4340 and 18 Ni, 200 grade maraging steels at the 200 ksi yield strength level are substantially improved by reducing the levels of impurity elements in the steels.

2) The predominate inclusion types in these alloys are ellipsoidal manganese sulfides in the AISI 4340 and cuboidal titanium carbonitrides in the 18 Ni, 200 grade maraging steel.

3) The average sizes of inclusions are larger in the commercial heats being studied while the actual numbers of inclusions per unit volume are greater in the high purity alloys.

4) The fracture toughness of these alloys is improved by reducing the average size of non-metallic inclusions in the structure.

5) The fracture of the 18 Ni, 200 grade maraging steel occurs by nucleation of voids at the carbo-nitrides and the subsequent growth and coalescence of these voids.

6) The fracture of the AISI 4340 alloy involves the nucleation and growth of two sets of voids, one set associated with the sulfide inclusions and one with the strengthening precipitates.

7) The fracture tends to follow ferrite boundaries in the AISI 4340 alloys while no definite microstructural path seems to be followed in the maraging alloys.

8) More work is needed to better understand the exact processes involved in the plastic fracture of these alloys.

REFERENCES

1. J. R. Low, Jr., Engr. Fract. Mech., 1 (1968) p. 47.

2. A. J. Birkle, R. P. Wei and G. E. Pellissier, Trans. ASM, 59 (1966) p. 981.

3. A. J. Birkle, D. S. Dabkowski, J. P. Paulina and L. F. Porter, Trans. ASM, 58 (1965) p. 285.

4. L. Roesch and G. Henry, Electron Microfractography, ASTM STP 453 (1969) p. 3.

5. D. M. Fisher and A. J. Repko, "Plane Strain Fracture Toughness Tests on 2.4- and 3.9-Inch Thick Maraging Steel Specimens at Various Yield Strength Levels," submitted for publication to Materials Research and Standards, Aug. 1971.

6. A. J. Baker, F. J. Lauta and R. P. Wei, Structure and Properties of Ultrahigh-Strength Steels, ASTM STP 370 (1965) p. 3.

7. J. M. Chilton and C. J. Barton, Trans. ASM, 60 (1967) p. 528.

8. R. Kiessling and N. Lange, Non-Metallic Inclusions in Steel, Part II, Iron and Steel Inst., London (1966) p. 97.

9. T. Boniszewski and E. Boniszewski, JISI, 204 (1966) p. 360.

10. R. T. DeHoff and F. N. Rhines, Trans. AIME, 221 (1961) p. 975.

11. R. T. DeHoff and F. N. Rhines, Quantitative Microscopy, McGraw-Hill, New York (1968) p. 145.

12. F. C. Hull and W. J. Houk, Trans. AIME, 197 (1953) p. 565.

13. E. J. Meyers, Proc. Fist. Int. Cong. Stereology, Vienna (1963) p. 151.

14. P. Hertz, Math Ann., 67 (1909) p. 387.

15. C. S. Smith, Trans. AIME, 218 (1960) p. 58.

16. E. E. Underwood, Quantitative Stereology, Addison-Wesley, Reading, Mass. (1970) p. 29.

17. K. H. Jack, JISI, 169 (1951) p. 26.

18. W. C. Leslie, R. M. Fisher and N. Sen, Acta Met., 7 (1959) p. 632.

REFERENCES (continued)

19. E. Tekin and P. M. Kelly, AIME Met. Soc. Conf., 28 (1965) p. 173.

20. A. M. Turkalo, Trans. AIME, 218 (1960) p. 24.

21. L. Roesch and G. Henry, ASTM STP 453 (1969) p. 3.